UCRL- 92721
PREPRINT

ASSESSMENT OF THERMAL DATA TO POLYMER MATERIALS BY FIRE PROPAGATION IN THE THREE MILE ISLAND UNIT 2 REACTOR BUILDING

N. J. ALVARES

THIS PAPER WAS PREPARED FOR SUBMITTAL TO
1985 AMERICAN CHEMICAL SOCIETY MEETING
MIAMI BEACH, FLORIDA
MAY 5, 1985

MAY 1985

Assessment of Thermal Damage to Polymeric Materials by Hydrogen Deflagration in the Three Mile Island Unit 2 Reactor Building*

N. J. Alvares**
Lawrence Livermore National Laboratory

UCRL--92721

DE87 008487

Thermal damage to susceptible material in accessible regions of the reactor building was distributed in non-uniform patterns. No clear explanation for non-uniformity was found in examined evidence, e.g., burned materials were adjacent to materials that appear similar but were not burned. Because these items were in proximity to vertical openings that extend the height of the reactor building, we assume the unburned materials preferentially absorbed water vapor during periods of high, local steam concentration. Simple hydrogen-fire-exposure tests and heat transfer calculations duplicate the degree of damage found on inspected materials from the containment building. These data support estimated 8% pre-fire hydrogen concentration predictions based on various hydrogen production mechanisms.

About 10 hours after the 28 March 1979 loss-of-coolant accident began at the Three Mile Island Unit 2 Reactor Building, a hydrogen deflagration of undetermined extent occurred inside the reactor building. Hydrogen was generated as a result of reaction between zirconium nuclear fuel rod cladding and steam produced as the reactor core was uncovered. Figures 1 through 4 are extracted from a variety of resources (indicated on figure), and they summarize

*This work was performed under the auspices of the U. S. Dept. of Energy by Lawrence Livermore National Laboratory under contract No. W-7405-ENG-48. Sections of this paper were originally published in GEND-INF-023, Vol. VI, U.S. Nuclear Regulatory Commission, Washington, D.C. (1983) under DOE Contract No. DE-AC07-76ID01570.

**I borrowed figures and paraphrased text from others (1, 3, 4) who devoted extensive time to analyze the hydrogen burn at TMI-2 reactor building. I acknowledge them throughout this paper, and I hope my interpretation of their analyses is correct.

the conditions and evidence of hydrogen release. Figure 1 is a schematic of the reactor coolant system showing the path of hydrogen release. Measurements of background activity increase (Figure 2) show the release occurred about 2.5 hours past turbine trip. Henrie and Postma (3) as well as Zalosh and others (1) estimate hydrogen accumulation in the core by a variety of means (Figure 3):

- o Timing of projected hydrogen generation in the core;
- o Timing the pressure relief valve opening periods;
- o Pressure changes in the reactor coolant system;
- o Calculations of hydrogen mass burned; and,
- o Measurements of post-burn hydrogen concentration.

Figure 4 shows the reactor-building pressure record starting from the time of reactor trip to well after the combustion produced pressure pulse.

Interviews with "on duty" plant personnel indicate they did not perceive that the "thud" they heard was caused by a hydrogen deflagration in the reactor building. Moreover, paucity of easily observable damage delayed recognition that a hydrogen burn did occur for about two days. Ignition of the hydrogen-and-air mixture release after the breach of the reactor coolant drain-tank (RCDT) rupture disk resulted in nominal thermal and overpressure damage to susceptible materials in all accessible regions of TMI-2. Initiation of burn and subsequent termination of induced fires are indicated by data from a variety of pressure and temperature sensors located throughout the containment volume.

Activation of the building spray system is defined by inflection and increase in the negative slope of interior-pressure-reduction curves (Figure 5). Also indicated is a pressure increase of about 28 psig achieved in a period of about 12 s.(3) Experimental confirmation of the pressure response of hydrogen combustion in constant volume chambers is indicated in Figure 6. Note that the act of causing turbulent conditions in the test chamber causes greater pressure rise at lower hydrogen concentration.

The hydrogen-in-air concentration [H_2] was estimated to be approximately 6 to 8%. At this concentration range, propagation of flame is possible upward and horizontally in quiescent conditions, but not downward. Figure 7 shows how laminar burning velocity varies with hydrogen concentration in air. Directed arrows at the lean and rich regions of hydrogen concentration indicate allowed flame-spread propagation vectors. This effect occurs because of competition between fundamental flame speed and buoyancy induced by reactants temperature rise. Figure 8 shows an example of lean limit propagation for methane-air-nitrogen mixtures. This illustrates the effect expected in hydrogen concentrations less than 8% in air. However, turbulent conditions, established circulation patterns, and the ambient absolute humidity of the mixture can perturb propagation patterns in ways that are only qualitatively understood.(4-5) Assuming uniform mixing of 8% hydrogen-in-air concentration and induction of adequate turbulence in internal circulation flows, average flame speeds of 5 m/s (16 ft/s) are possible -- even in the presence of saturated steam environments.(6)

A cross section of the reactor building (Figure 9) and plan view of the main (347-ft) operations level (Figure 10) show the regions of thermal and burn damage. Given that few operational ignition sources were available in the reactor building above the 305-ft level, the time delay to achieve peak overpressure is consistent with an ignition location in the basement. Potential electrical shorting of electrical control systems caused by basement water spillage and the frequency of steam and hydrogen release from the reactor coolant drain-tank pressure-release system supports this assumption.

Thermal damage to fine fuels (fine fuel is defined as a flammable material with high surface-to-volume ratio) indicates general exposure of all susceptible interior surfaces to fire with the exception of random materials including fabric ties of unknown composition, 2 x 4 framing lumber on both the 305-ft and 347-ft levels, and various polymeric materials. These unburned items are evident in photographic and video surveys, and were visually reconfirmed by various entry participants. This pattern is reported in several preliminary reports.(7-8) Possible mechanisms to prevent thermal damage to these items include:

- Preferential absorption of water from saturated atmosphere, requiring greater thermal exposure to produce thermal damage.
- Direct exposure to high-concentration steam and water vapor, requiring greater thermal exposure to produce thermal damage.
- Shielding from thermal radiation by position or geometric obscuration.
- Shielding from the expanding flame front or convectively driven hot gases by physical obstruction.

Although photographic surveys of internal reactor building vistas, ensembles, items, and surfaces were abundant (approx 600 photos from 29 entries), clarity of the burn detail in most photographs was not adequate for diagnostic purposes. However, the extent of thermal damage was defined (Figures 9 and 10) as regions where thermally degraded materials were located, photographed, and, in some cases, extracted from the reactor building for further examination.

Ignition of a uniformly distributed near-lower-limit mixture of hydrogen in air, spreading from basement ignition sources to the top of the reactor building dome by turbulent propagation modes, occurred in the time period indicated in Figure 5. The flame front would have been at an adiabatic flame temperature of about 700°C to 800°C (approximately 1000°K), as shown in Figure 11.

Exact paths of flame propagation are undefined. Because of the low hydrogen concentration, preferential flame spread was upward in quiescent atmosphere; however, air motion produced by reactor building coolers, steam/hydrogen release from the rupture disk line of the RCDT and flow distortion around obstructions caused turbulent flow conditions which greatly modify flame spread

rates. The source of major hydrogen release was located near the open stairway on the undersurface of the 305-ft level plane (Figure 12). Henrie and Postma (3) conclude that the primary path for entry of the hydrogen-and-steam mixture to the total reactor building above the basement (282 ft) level was through this stairwell. How these gases from the rupture disk line interacted with total ventilation patterns is not known. This may be a moot point since, by the time ignition occurred, hydrogen in the reactor building was substantially mixed.

Identification of a specific ignition source is not possible from available documentation; however, two potential basement source-types are considered. (1) Several circuit boxes, instrument racks, meters, and control components were at various locations around D-rings and containment walls at undefined heights above the basement floor. Failure of circuit components may have been caused by immersion in water. (2) Plant operators who control core and reactor building conditions may have produced ignition arcs from control components perturbed by thermal or mechanical effects of reactor excursion.(2) The inner perimeter of the reactor building basement had no obstructions to block or blind flow of gases outside of the D-ring. However, there were constrictions that could temporarily horizontal hydrogen mixing in the basement.(1) Approximately 10% of the cooled gases from the cooling system plenum (25,000 ft^3/min) was distributed to the basement (outside of the D-ring) through committed ducting. The only exit paths for these gases were the 4-in. seismic gaps, a space that physically separates each floor level from the reactor building, many pipe penetrations and the open stairwell that extended from the basement space to the 347-level without barrier. (A recently identified path for hydrogen release is the in-core instrumentation cable chase which provides a large open area between the basement and the 305-ft level.(12)) If ignition occurred at sources away from the open stairwell, the preferred flame propagation would be upward through the seismic gap, and above the 305-ft level, through the grating in the 347-ft level floor. Horizontal spread would occur, but at a slower rate, even during turbulent propagation conditions. Ample evidence exists on the 347-ft level to confirm flame propagation through the seismic gap regions and the floor grating.

At the peak pressure rise of about 28 psig during the hydrogen burn, the adiabatic temperature rise during combustion of 6 to 8% hydrogen-in-air mixture is about 1000°K. At this temperature, calculated exposure radiative and convective flux ($\dot{q}_t$) from an optically thick combustion plume is

$$2.2 \text{ W/cm}^2 < \dot{q}_t < 4.5 \text{ W/cm}^2 .$$

This range is approximate because we assume values for combustion zone emittance (ε) at limits of the range $0.2 < \varepsilon < 0.8$. It is quite possible that ε could be larger for optically thick hydrogen combustion zones.(9) Figure 13 compares radiant emission from methane/air fires at various plume diameters. As zone volume increases, the product of emittance times absolute temperature correspondly increases. Since plume temperature is essentially constant, their flame and hot gas emittance is shown to be directly

proportional to gas volume. Heat transfer coefficient for minimum and maximum convective heat transfer is based on gas velocity (u_g) at the limits of the range:

$3 \text{ m/s} < u_g < 12 \text{ m/s}$.

Examination of TMI Materials

To estimate the intensity of thermal exposure to damaged materials and to analyze thermal damage patterns, it is necessary to examine their condition and to determine their composition. Photographic evidence is inadequate for such appraisal. We examined materials removed from the reactor building, and recommended removal of additional materials for analysis. We examined the following materials (available July 1983):

Level 305	Level 347	Polar Crane
Polypropylene bucket	Plywood board	Fire extinguisher
	Wood from tool box	Hypalon polar crane pendant jacket control box
	Two radiation signs, probably polyethylene	
	Hemp and polypropylene rope	
	Catalog remains	
	Telephone and associated wire	

These materials retain residual radioactive contamination. Consequently, all examinations were performed under radiologically-safe conditions. Chemical or physical analytical procedures could only be done with contaminated or easily decontaminated instruments. We were unable to locate expendable diagnostic equipment; therefore, our examination of extracted materials was limited to detailed photography and macroscopic observations.

Figure 14 shows photographs of plywood on the reactor building south wall and remains of an instruction or maintenance manual located on the reactor building north wall, both ignited by fire propagation through the seismic gap and/or radiant exposure from combustion gases in reactor building free volume. In Figure 14(a) note the wires along the wall also exhibit burn trauma. Figures 14(c) and 14(d) show the front and rear surface of the plywood panel after it was extracted from the south wall of the reactor building, over the seismic gap. Both sides are charred, as are edges and holes through which wire ties penetrate. Surface char condition indicates the panel ignited to flaming combustion for a short period before self-extinguishing or being quenched by the reactor spray system. Regardless of the ignition source location, it is apparent that a hydrogen-and-air flame front

traversed most of the reactor building volume above (and probably below) the 305-ft level. Duration of this propagation was about 12 s. Slow temperature decay before operation of the building spray system ensured thermal exposure to combustible or thermally sensitive surfaces was sufficient to produce thermal damage and/or ignition of these materials, particularly in regions where volume of the combustion plume was optically thick.

The pendant and festoon for the polar crane possibly received the most intense energy exposure. The covering of this cable is Du Pont Hypalon and ethlylene propylene rubber. Figures 15(a) and 15(b) show the lower polar crane pendant, and upper polar crane pendant and festoon along the "A" girder of the crane. Figures 15(c) and 15(d) show the relative thermal damage of cable sections extracted from the reactor building. (This examination was conducted at Sandia Laboratories, Albuquerque, in cooperation with Mr. Ralph Trujillo, Project Manager for the cable integrity project for TMI-2 reactor building electrical circuits.(10)) A detailed description of thermal damage on each section is contained in Figure 16, along with a curve showing β/γ activity along the pendant cable. Figures 15 and 16 show that all sections received thermal exposure, including those coiled on the D-ring catwalk. The degree of thermal degradation decreased from the polar-crane level to the D-ring top, and, in fact, was only apparent on the bottom pieces where cuts in insulation projected free surfaces of poor heat transfer. Thermal degration is also apparent on light lenses of the pendant control box.

Maximum thermal damage occurs in the region from 6 to 10 ft below the polar crane girder (from about the 440-ft level down to about the 406-ft level). This region shows locally high β/γ activity, which may correlate to physical absorption by porous, charred insulation. Thermal damage is severe and circumferentially equal in this region. Char depth on the polymer surface averages 1 to 2 mm.

From the 406-ft level to the top of the D-ring (the 367-ft level), thermal damage is progressively less and becomes more directional, i.e, half of the insulation circumference exhibited a heavier degree of damage, ranging from char at the 406-ft level to no perceptible insulation degradation just above the D-ring plane. The pattern of asymmetric thermal damage along the pendant below the 406-ft level (a distance approximately 14 ft below polar crane girder bottom) indicates exposure from a westerly direction.(10) The extent of thermal damage to other available polymers at about the 347-ft level indicates intense thermal exposure in southerly areas of the reactor building. Morever, since all containment gases above the 347-ft level were convected to the air-cooler intake plenums in the southern sector just below the 347-ft level, some preferential ventilation pattern may have influenced fire propagation path. However, because of fewer thermally susceptible materials in the north reactor building regions, we cannot confidently compare the south and north experience to define sources of non-uniform heat flux. Had there been either minimal thermal experience or other patterns in susceptible polymers in any other region, we may have had better opportunity to define fire geometry. One cause for asymmetry of the burn pattern below the 406-ft level can be conjectured: the cable at this height was

exposed to radiation and convection resulting from hydrogen combustion originating from one side (logically the southwest side) of the reactor building. The exposed surface would sustain thermal damage more readily than the shadowed surface, thus producing the observed pattern.

Photographic documentation of thermal damage patterns sustained by items removed from the TMI-2 reactor building revealed a variety of responses from different materials located in the same general area, e.g., materials around the telephone on the south reactor building wall of the 347-ft level show quite a different response relative to material composition.

Thermal Measurements on Exemplar Materials

To augment this analysis, we located exemplar materials generally similar to those removed from the reactor building. Response properties of the exemplar materials were measured in a thermal gravimetric analyzer (TGA) to ascertain the temperature range of thermal degradation and weight-loss rates. Figure 17 shows TGA patterns for ABS, acrylonitrile butadiene styrene, a standard material from the National Bureau of Standards (NBS) used as a control for smoke tests. ABS is similar to telephone body material.

Thermograms are obtained by isothermally heating milligram-sized samples of materials, supported on a micro balance, at a constant temperature rate. Weight loss with temperature indicates thermal degradation mode and mechanism. The temperature range of maximum weight loss indicates critical conditions for producing potentially ignitable pyrolyzates. Figure 17 shows that NBS-ABS flammable pyrolyzates are produced in the temperature range of 370° to 500°C, leaving about 20% inert materials as residue. These pyrolyzates are flammable which, with an external ignition source, will ignite within this range.

The temperature corresponding to the median of weight loss during the first major weight-loss experience in any polymer can be used to estimate the condition where the rate of thermal destruction is maximum, as in the case of pyrolyzate production. Thus, we can use this temperature to define the time when subject materials are most susceptible to ignition.

Using standard solutions for transient heat conduction in semi-infinite solids with constant thermal properties, it is possible to calculate the time at which a material's surface will attain a specific temperature upon exposure to constant thermal flux levels. Adjustments should be made to account for re-radiation heat losses from exposure surfaces and latent heat processes required to produce pyrolyzates from polymers. With specific surface temperature, exposure heat flux, and defined thermal constants, the time required to reach this temperature is determined by solution of the differential equation for transport heat flow in a semi-infinite solid:

$$t = \left(\frac{\pi T_s}{2\dot{q}_t}\right)^2 k\rho c_p \quad , \qquad (1)$$

where

$\dot{q}_t$ = total thermal exposure,

T_s = surface temperature,

$k\rho c_p$ = material thermal constants.

Times calculated using this equation should be short relative to those for real materials which experience both thermal and mass convection heat losses. To account for these losses, we adjust q_t by subtracting from it the surface radiation energy at the specified critical surface temperature and the mass convection losses (the product of surface mass loss and latent heat of pyrolysis). The resultant effective energy exposure rate $\dot{q}_e$ replaces $\dot{q}_t$ in Equation 1, giving a longer time to attain the critical temperature level. Values for time obtained by using both $\dot{q}_t$ and $\dot{q}_e$ in Equation 1 bound the time range between exposure of an inert solid and a solid experiencing both re-radiation and latent heat losses. Critical temperature for the three materials is estimated to be 600°K, and thermal exposure energy is the high value calculated from both convective and radiative exposure during combustion of 8% hydrogen in air ($\dot{q}_t$ = 4.5 W/cm^2).

These materials and times to critical weight-loss are

Material	$t_e(\dot{q}_t)$	$t_c(\dot{q}_e)$
Pine wood	5.3 s	9.4 s
PVC	32.0 s	54.7 s
Acrylic	40.0 s	68.0 s.

Times to attain critical temperature conditions in these materials are of the same order of duration as those recorded during the hydrogen burn in free volumes of the reactor building. Thus, all susceptible materials exposed to this energy should (and did) experience thermal degradation and/or flaming ignition.

Hydrogen-Fire-Exposure Tests

Thermal constants of most polymeric materials are defined only for virgin compounds. It is virtually impossible to calculate thermal response properties of commercially available polymers because additives, retardants, and fillers modify fundamental properties; however, simple hydrogen-fire-exposure tests may give an indication of accident exposure conditions. To assess this possibility, we conducted selected exposure tests on our exemplar materials using a Meeker burner adjusted to a fully pre-mixed burning mode.(11) Flow was adjusted to produce a measured flame temperature of 833°K (note: during measurement, the 20-mil thermocouple was incandescent, so measured temperature was substantially lower than actual flame temperature). A simple-copper-slug calorimeter measurement of total thermal flux indicated an exposure flux of 6 W/cm^2. This level of flame temperature and thermal flux was within reasonable limits of projected TMI-2 accident measurements and estimated reactor exposure conditions. Thus, resulting data trends should be similar to thermal response variations of materials that suffered hydrogen-flame exposure in the TMI-2 reactor building.

Table I lists results of small-scale hydrogen-exposure tests. Note the time to significant thermal damage is well within times to critical exposure calculated herein. Similarity of thermal damage sustained by materials from the reactor building and those used in the small-scale test were encouraging. Both duration and intensity of test thermal exposure is in the range of estimated thermal fluxes extant during the reactor building burn. Note that these are very simplistic tests. No attempt was made to refine temperature or thermal energy measurement. We have no illusion as to the distribution of convective or radiative contribution from the test burner; however, the results give data trends which are intuitively acceptable.

Conclusions

On the basis of

- photographic and video surveys of the TMI-2 reactor building interior,
- visual and photographic analysis of materials extracted from the reactor building,
- macro- and micro-experiments with materials of composition generically similar to that of extracted TMI samples, and
- calculations using proposed physical conditons and assumed material properties,

the following conclusions are posed:

1. Hydrogen concentration in the reactor building prior to burn burn is confirmed to be about 8%, as calculated by analyzers of TMI-2 pressure and temperature records.
2. No preferred path for hydrogen flame propagation has been established, and there is no evidence to preclude hydrogen deflagration throughout the entire free volume of the reactor building.
3. The most probable ignition site for the hydrogen burn is in the basement volume outside of the D-ring: radial location is not defined.
4. Thermal degradation of most susceptible materials on all levels is consistent with direct flame exposure from hydrogen fire.
5. The directional character of damage to lower pendant length suggests potential geometric limitation of the hydrogen-fire propagation paths.
6. The total burn pattern of the plywood tack board for the south-wall telephone on the 347-ft level indicates flame

propagation through the seismic gap.

7. Lack of thermal degradation to some thermally susceptible materials at the 305-ft and 347-ft levels may result from preferential moisture absorption, relative to thermally degraded materials at adjacent locations. Because of the random nature of this evidence, it is not likely that lack of damage resulted from selective shadowing.

8. Burn patterns in the reactor building indicate that the dome region above the 406-ft level was uniformly exposed to direct hydrogen combustion and high heat flux for the longest duration. The region between the 406-ft level and the top of the D-ring was exposed to directional heat flux (most likely from the south and west quadrants); and, the damage on the 305-ft level was geometrically similar to that above the 347-ft level but less severe.

Table I. Results of Hydrogen-Fire-Exposure Tests on Exemplar Materials

Sample	Test	Time (s)	Energy exposure (J/cm^2)	Results of exposure
Polypropylene rope	1	12	72	Melted at ends, waxy
"	1A	30	180	More melting at ends than test 1, some blending of materials
"	1B	27	162	Melting at point of contact, breakage occurred at 27 s into test with moderate pulling force applied
"	1C	33	198	More melting than test 1B, breakage occurred at 33 s into test with very little force applied
Telephone receiver cord	2	12	72	Melting, fusing of jacket, conductors exposed, bubbling of clear plastic plug
	2A	30	180	More melting of jacket than test 2, char formation, signs of dripping, conductors exposed and ignited at 29 s into test
Telephone dial	3	12	72	Melting at edges, some bubbling
	3A	20	120	Melting at edges, incipient bubbling
Telephone dial (on screen)	4	30	180	(Material placed on screen to prevent dripping onto burner): Melted into screen, bubbling
"	4A	20	unknown	(Inadvertent flame temp decrease approx 30-40°C): Bubbling
"	4B	35	unknown	(Inadvertent flame temp decrease approx 30-40°C): More bubbling than 4A

Table I. Results of Hydrogen-Fire-Exposure Tests on Exemplar Materials (continued)

Sample	Test	Time (s)	Energy exposure (J/cm^2)	Results of exposure
Telephone extension line	5	12	72	Melting, charring along edge of cable, bubbling and deformation of clear plastic plug
	5A	20	120	More charring and melting than in test 5; ignited approx 18 s into test
Plywood	6	12	71	Some charring along edges
	6A	20	120	More charring than in test 6, minimal buring through top lamina
	6B	30	180	More charring of top surfaces, outer edges, and corners; splitting of top layer
	6C	60	360	Extreme charring of top surfaces and sides; ashy appearance at corners
Plywood (wet)	7	12	72	No noticeable change
	7A	30	180	Slight char along one edge
	7B	60	360	Charring approx like test 6B
ABS (white material)	8	12	72	Loss of strength; bubbling, slight char, deformation
"	8A	20	120	More bubbling, deformation, blackening of approx 74% of surface area
ABS (on screen)	8B	30	180	More bubbling, melted edges, melted into screen, brownish color over surface
"	8C	40	240	"

Table I. Results of Hydrogen-Fire-Exposure Tests on Exemplar Materials (continued)

Sample	Test	Time (s)	Energy exposure (J/cm^2)	Results of exposure
Duct tape	9	12	72	Widespread bubbling, penetration through top (silver) layer
"	9A	20	120	More bubbling than in test 9, penetration through top layer
"	9B	30	180	More bubbling, charring, melting of adhesive; penetration through top layer
Plywood covered with PE	12	12	72	Plywood covered with single layer of polyethylene one side only: PE burned completely away, charring on 2 opposite edges
"	12A	12	72	Plywood covered with double layer of PE on one side only: 25% of PE lost due to drippage and shrinkage; charring along edges of plywood
"	12B	20	120	Double layer of PE on one side of plywood: PE burned completely away; charring at edges and corners of plywood; PE ignited at 15 s into test and one edge of the plywood ignited also
"	12C	12.5	75	Wood placed in PE bag: Bag burned away at approx 7 s; noticeable color change in wood at approx 12.5 s
"	12D	9.5	57	Plywood placed in PE bag: Bag burned away approx 6 s into test; noticeable color change in plywood at approx 9.5 s
"	12E	13	78	Plywood placed in PE bag: Bag burned away approx 6 s into test; noticeable color change in plywood at approx 13 s (this plywood was a darker piece than used in test 12D)

Table I. Results of Hydrogen-Fire-Exposure Tests on Exemplar Materials (continued)

Sample	Test	Time (s)	Energy exposure (J/cm^2)	Results of exposure
Telephone body	10	12	71	Loss of strength, some wrinkling
"	10A	20	120	Leathered appearance, bubbling
"	10B	30	180	More bubbling; otherwise same as test 10A
Hose	11	12	72	No noticeable change
"	11A	20	120	No noticeable change
"	11B	30	180	Some discoloration
"	11C	60	360	Charring, slight deformation, melting of outer covering

Literature Cited

1. Zalosh, R. G., et al. "Analysis of the Hydrogen Burn in the TMI-2 Containment"; EPRI NP-3975 Project 2168-1, Final Report, April 1985.
2. VanWitbeck, T. L.; Putman, J. "Annotated Sequence of Events, March 28, 1979"; GPU Nuclear, TDR-044 (1982).
3. Henrie, J. O.; Postma, A. K. "Analysis of the Three Mile Island (TMI-2) Hydrogen Burn"; Rockwell International, Rockwell Hanford Operations, Energy Systems Group, Richland, WA, RHO-RE-SA-8 (1982).
4. Hertzberg, M. "Flammability Limits and Pressure Development in H_2-Air Mixtures"; Pittsburgh Research Center, Pittsburgh, PA, PRC Report No. 4305 (1981).
5. "Flame and Detonation Initiation and Propagation in Various Hydrogen-Air Mixtures, With and Without Water Spray"; Rockwell International, Atomics International Division, Energy Systems Group, Canoga Park, CA, A1-73-29.
6. Lowry, W. E.; Bowman, B. R.; Davis B. W. "Final Results of the Hydrogen Igniter Experimental Program"; Lawrence Livermore National Laboratory, Livermore, CA, UCRL-53036; U. S. Nuclear Regulatory Commission, NUREG/CR-2486.
7. Eidem, G. R.; Horan, J. T. "Color Photographs of the Three Mile Island Unit 2 Reactor Containment Building: Vol.1 Entries 1, 2, 4, 6"; U. S. Nuclear Regulator Commission, Washington, DC, GEND 006 (1981).
8. Alvares, N. J.; Beason, D. G.; Eidem, G. R. "Investigation of Hydrogen Burn Damage in the Three Mile Island Unit 2 Reactor Building"; U. S. Nuclear Regulatory Commission, Washington, DC, GEND-INF-023 Vol. 1 (1982).
9. Hertzberg, M.; Johnson, A. L.; Kuchta, J. M.; Furno, A. L. "The Spectral Radiance Growth, Flame Temperatures, and Flammability Behavior of Large-Scale, Spherical, Combustion Waves"; Proc. 16th Symposium (International) on Combustion, The Combustion Institute, Pittsburgh, PA (1976).
10. Trujillo, R.; Cannon, P. "Cable/Connections Task: Report No. 1 Polar Crane Pendant Cable," unpublished report.
11. Lewis B.; von Elbe, G. "Combustion, Flames and Explosions of Gases"; 2nd ed. Academic Press: New York, 1961; p. 490.
12. Zalosh, R. G., personal communication.

*This work was performed under the auspices of the U.S. Department of Energy by Lawrence Livermore National Laboratory under contract No. W-7405-Eng-48.

Figure 1. Reactor coolant system schematic showing hydrogen release path through reactor coolant drank tank (1).

Figure 2. Background activity as measured by sensor in dome (2).

Figure 3. Hydrogen production estimates based on analysis of pre- and post-burn core and reactor building indicators (3).

Figure 4. Reactor building pressure record (1).

Figure 5. Pressures recorded during the burn from OTSG (once-through steam generator) pressure transmitters and pressure switch actuation times (1). Corresponding average temperature via procedure described in Ref.1 added to psig scale.

Figure 6. Pressure rise (Δp) produced by burning hydrogen ignited in constant volume chambers (4).

Figure 7. Flame speed of varying hydrogen in air mixtures (4).

Figure 8. Lean methane and nitrogen in air mixture flame propagation patterns (6.9% CH_4 - 27.3% N_2 65.8% Air) (4).

Figure 9. Cross section of TMI-2 reactor containment building (7).

Figure 10. Thermal and burn damage and potential overpressure on the 347-ft level (7-8).

Figure 11. Temperature rise produced by combustion of pre-mixed hydrogen and air (3).

Figure 12. Schematic of reactor basement geometry showing relation of reactor coolant drain tank to relative gas distribution patterns (1).

Figure 13. Emittance vs fire depth (9).

Figure 14. Hydrogen-burned in-containment materials. (a) Bell telephone at TMI; (b) Charred manual on electrical box; (c) Plywood panel (back); (d) Plywood panel (front).

Figure 15. In-containment views and sectional pieces of the polar crane pendant: (a) Job crane; D-ring A is in lower right; (b) Girder A of the polar crane; (c) North side of cable is ash; plastic tape is charred all around; no degradation under the tape; (d) Half of circumference is ash, half char (ash is gray; char, black).

Figure 16. Thermal damage pattern and β/γ activity along the Du Pont Hypalon and ethylene propylene covered polar crane pendant.

Figure 17. Thermogram of NBS-ABS. In air, 20°C per min heating rate.

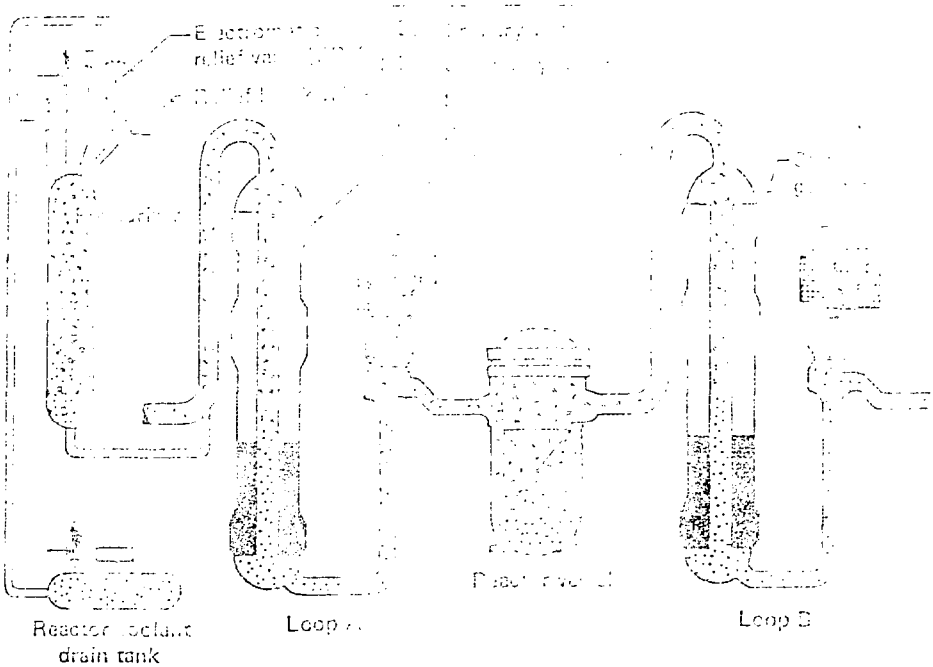

Fig. 1

Fig 1

Fig. 2

Fig 2

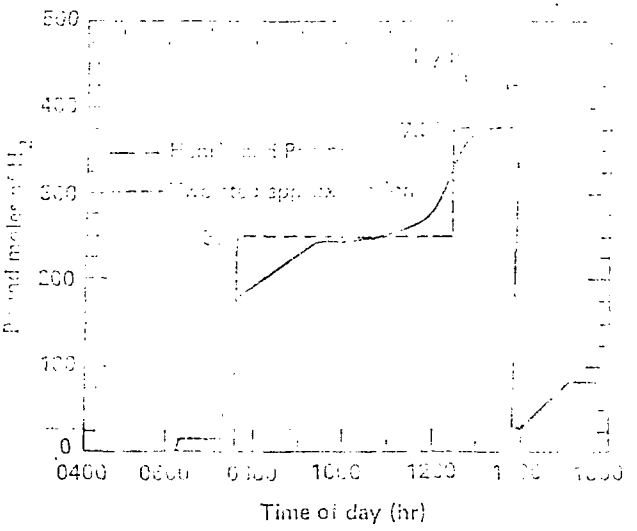

Fig. 3

Fig 3

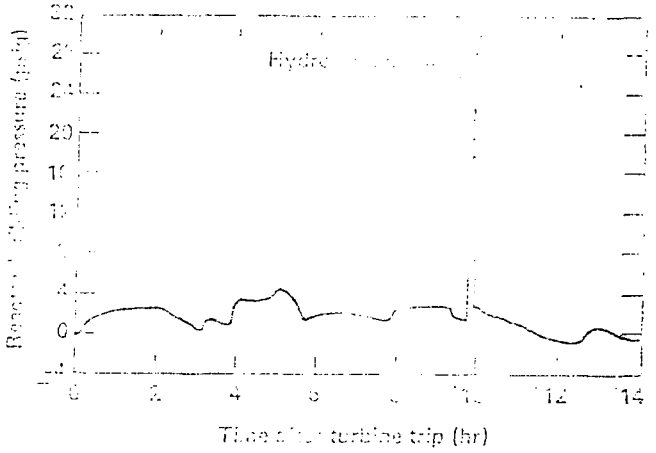

Fig. 4

Fig 4

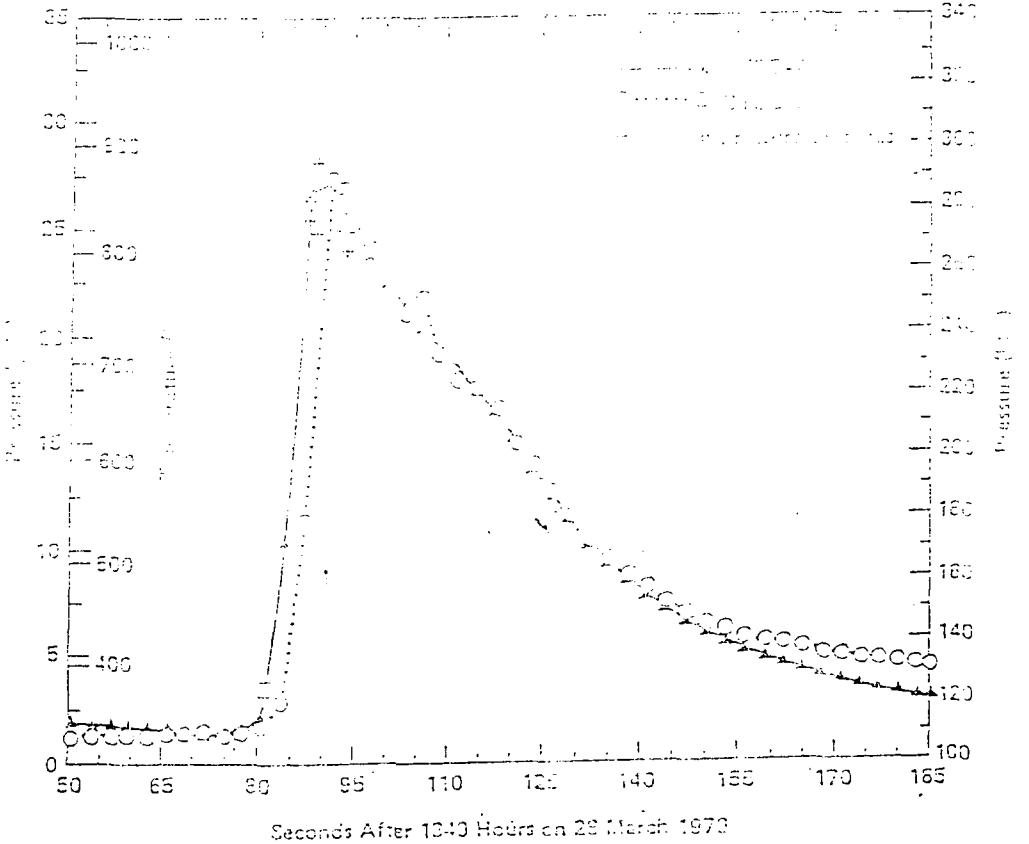

Fig. 5

Fig. 5. Pressures recorded during the burn from OTSC pressure transmitters and pressure switch actuation times. Corresponding average temperature via procedure described in Ref. 1 added to psig scale.

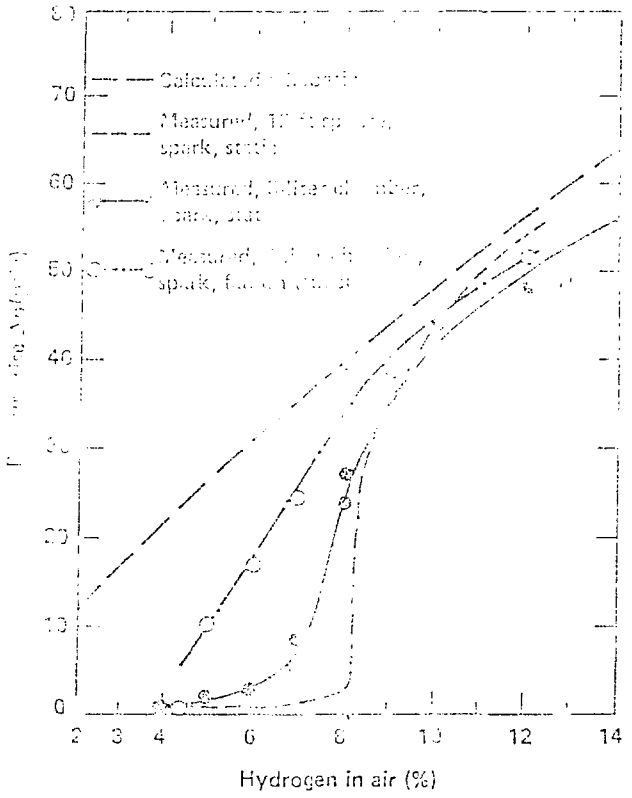

Fig. 6

Fig. 6

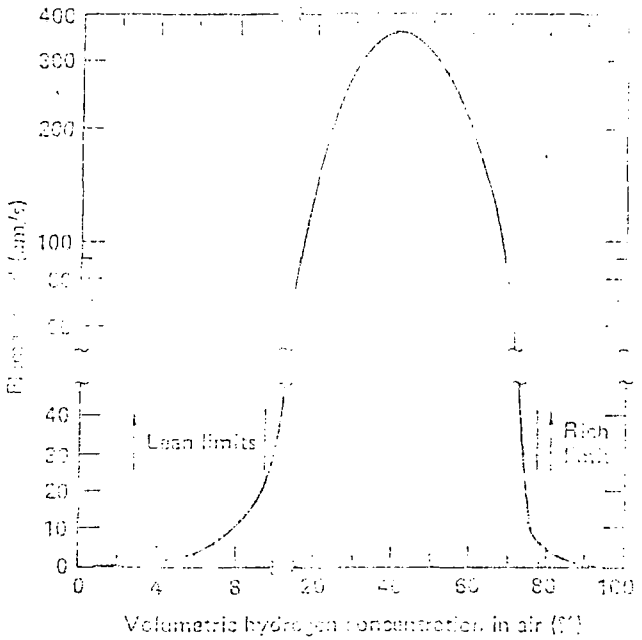
400
300
200
100
40
30
20
10
0
Lean limits
Rich
0
4
8
20
60
80
100
Volumetric hydrogen concentration in air (%)

Fig. 7

Fig. 8

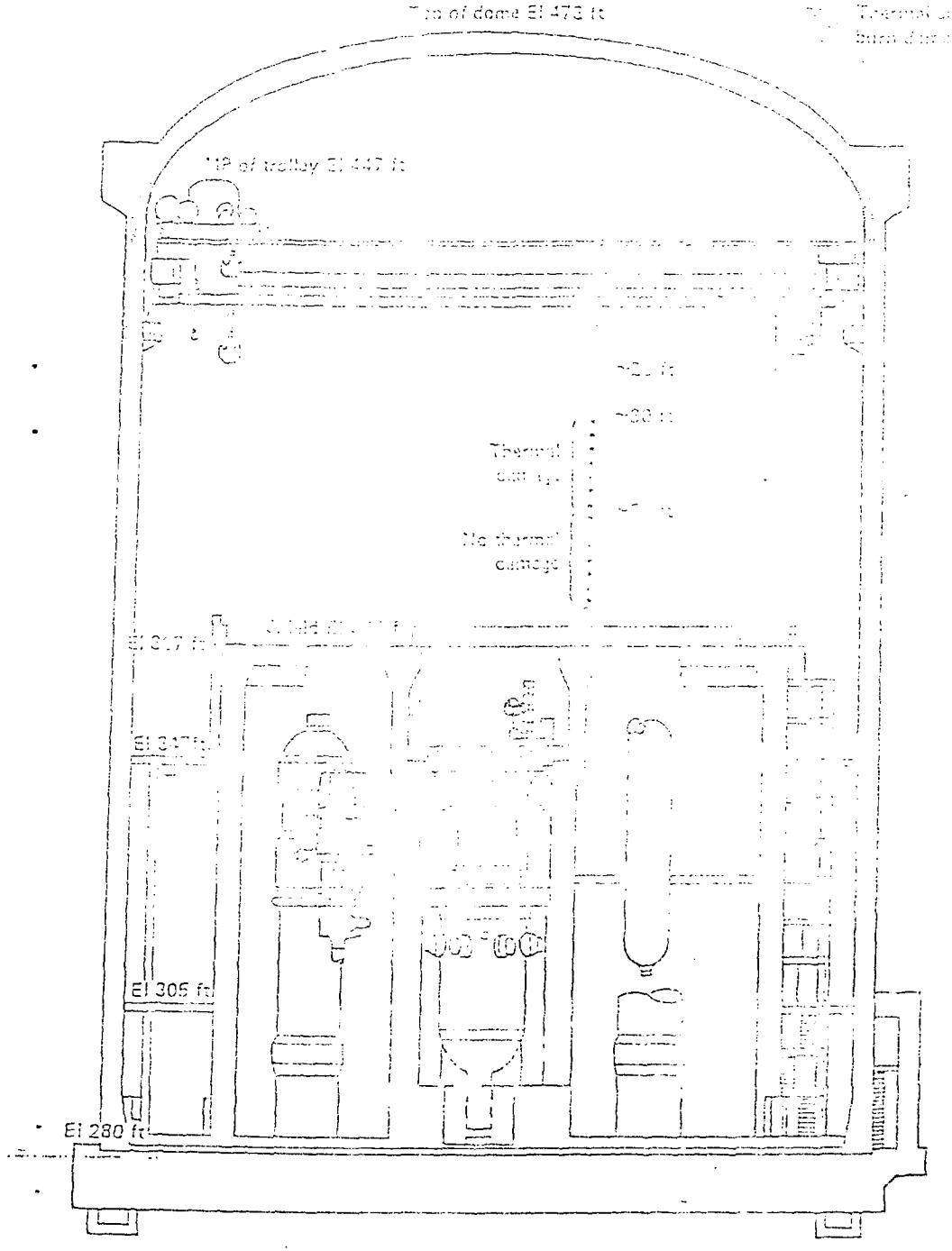

Fig. 4. Cross section of the TMI-2 reactor containment building.

Fig. 9

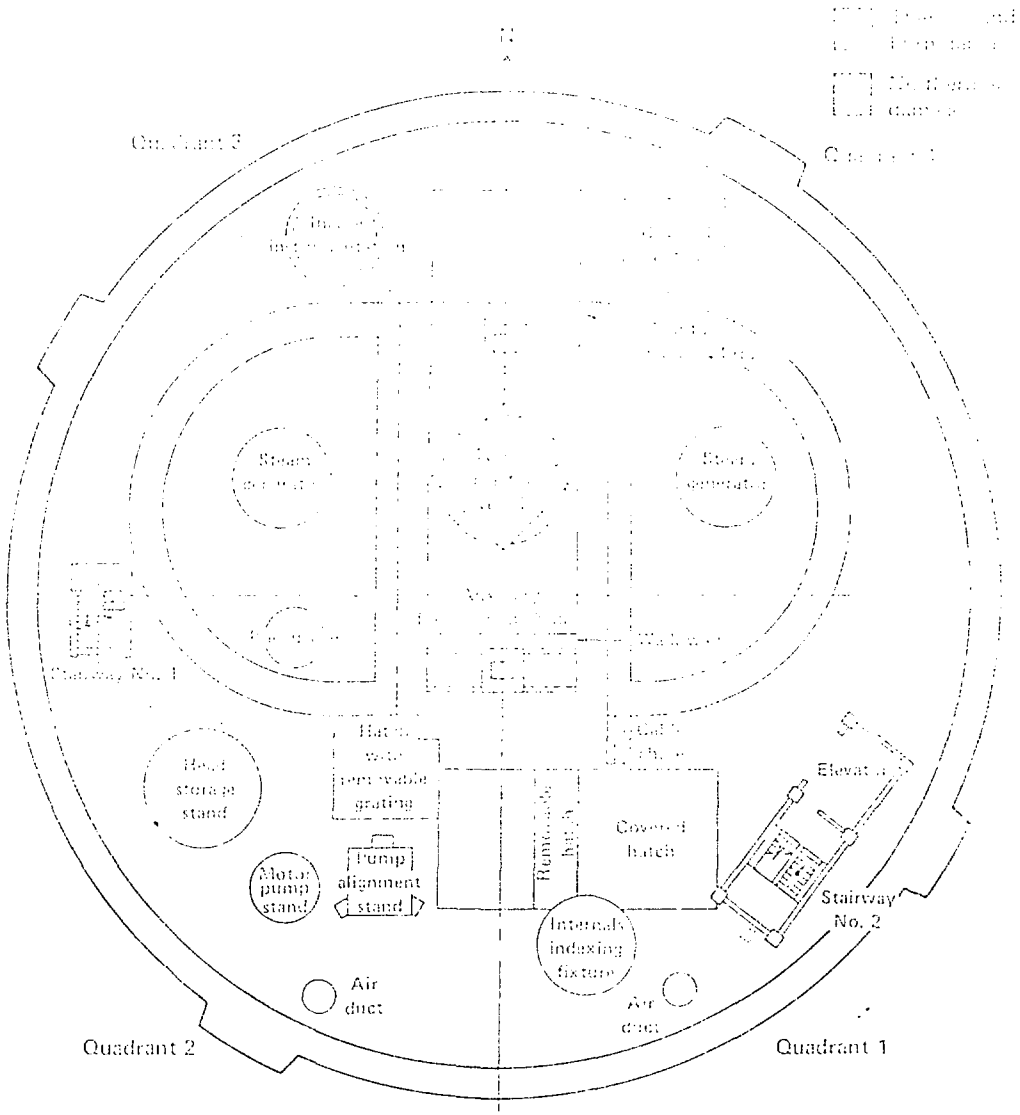
Stairway No. 1
Head storage stand
Motor pump stand
Pump alignment stand
Internals indexing fixture
Covered hatch
Elevator
Stairway No. 2
Air duct
Air duct
Quadrant 2
Quadrant 1

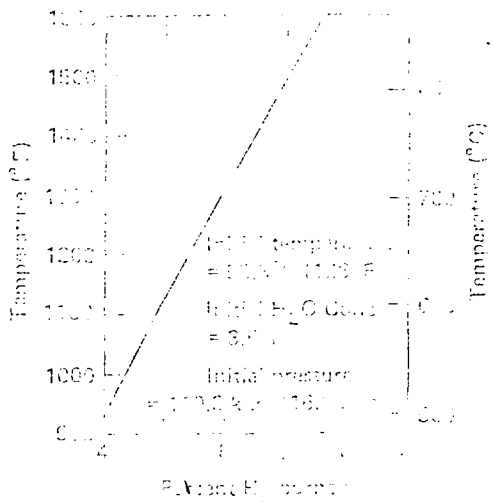

Fig. 11

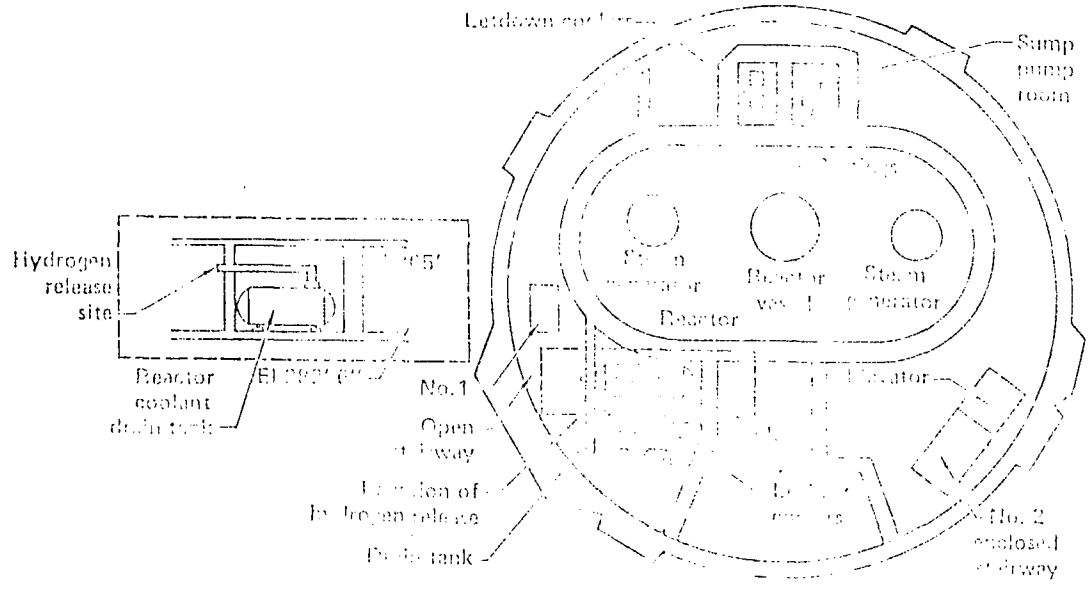
Sump pump room
Hydrogen release site
Reactor coolant drain tank
No. 1
Open
Reactor
Steam
No. 2
enclosed

Fig. 12

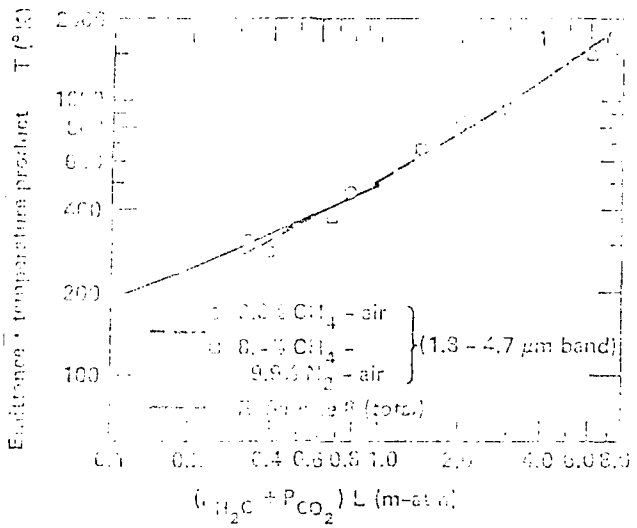
Equilibrium temperature product T (°K)
400
200
100
0.1
0.4
0.6
0.8
1.0
4.0
6.0
8.0
(P_H2O + P_CO2) L (m-atm)
- air
(1.3 – 4.7 μm band)

Fig. 13

(a) Fall end plate at TMI

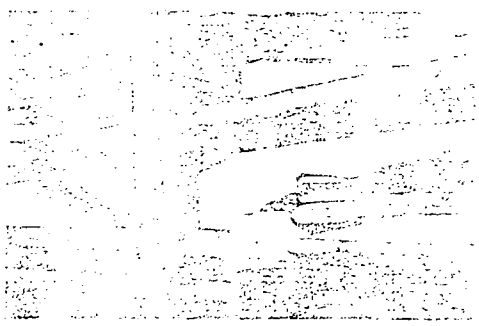

(b) [illegible] on elevator

(c) Plywood panel (back) extracted from TMI

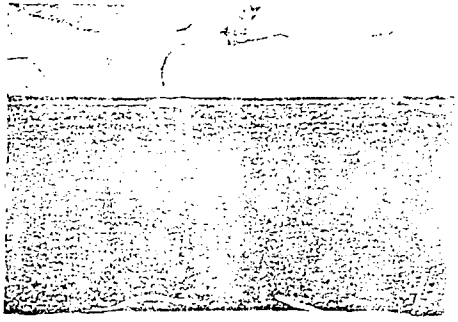

(d) Plywood panel (front) extracted from TMI

14

Fig. 14. Hydrogen-burned in-containment materials.

Fig. 14

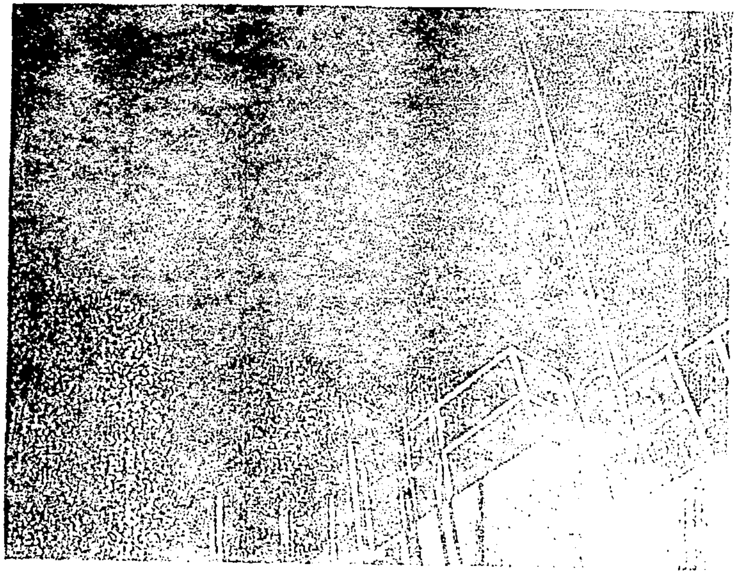

a

Jib crane; D-ring A lower right.

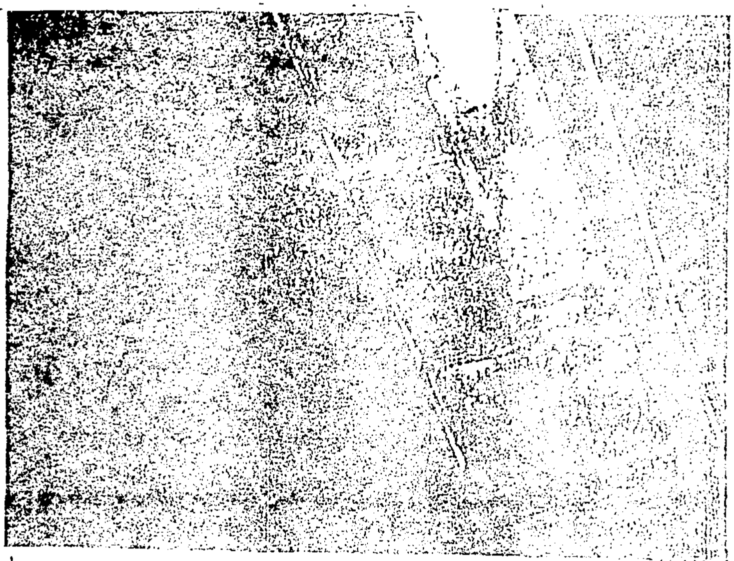

b

Girder A of the polar crane.

Fig. 15

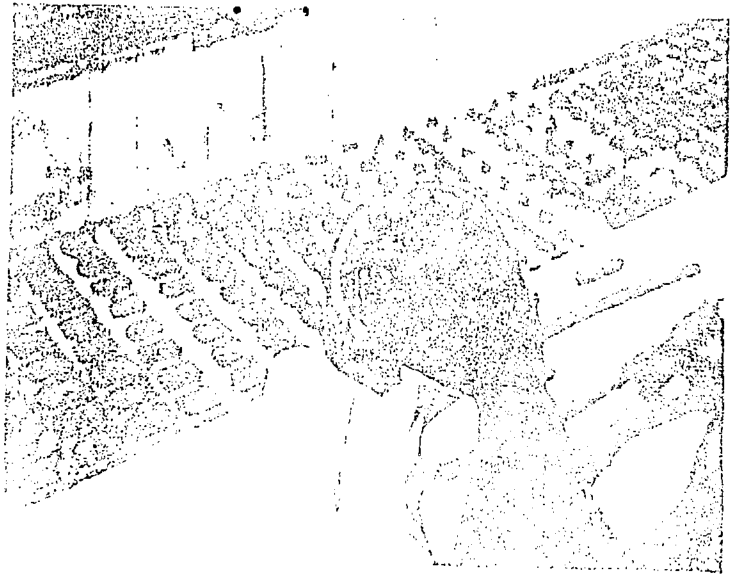

31. [illegible]

30. [illegible]

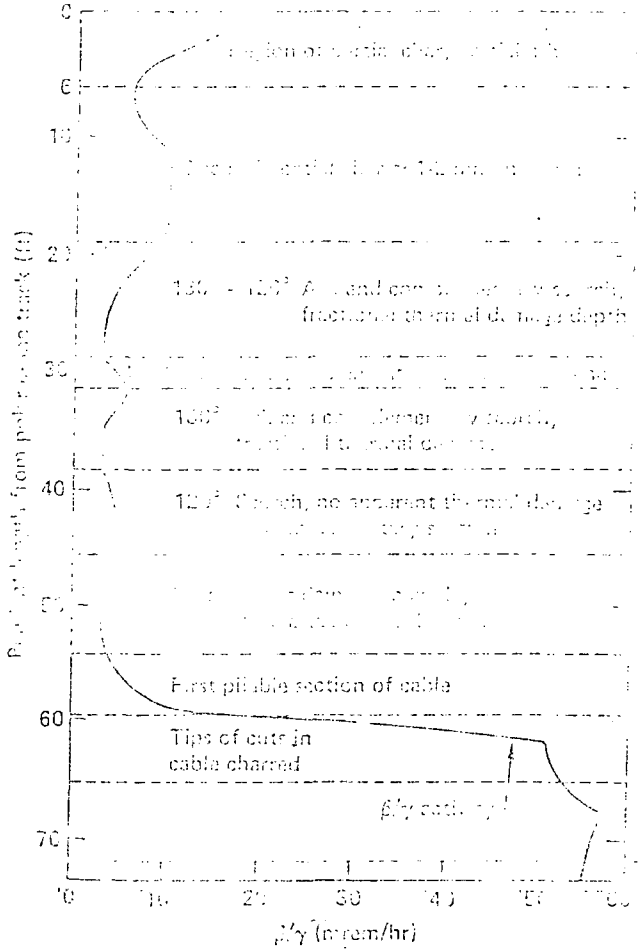
0
6
10
20
30
40
50
60
70
First pitable section of cable
Tips of cuts in cable channel
β/γ cable
β/γ (mrem/hr)

Fig. 14

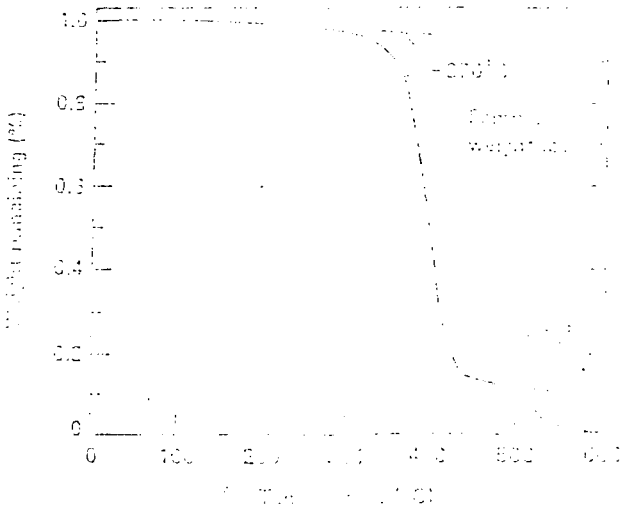

Fig.17